

1 ELECTRONIC SUPPLEMENTARY INFORMATION

2 **Ligand-Binding Assay Based on Microfluidic Chemotaxis**  
3 **of Porphyrin Receptors**

4  
5 Bin Li,<sup>‡a</sup> Kejiao Gao,<sup>‡a</sup> Yurong Li,<sup>a</sup> Yuansheng Li,<sup>a</sup> Longyi Zhu,<sup>b,\*</sup> Xuanyu Fu,<sup>a</sup> Xiyong Zhuo,<sup>a</sup>  
6 Ying Wu,<sup>a</sup> Ying Wan,<sup>\*c</sup> and Shengyuan Deng<sup>\*a</sup>

7  
8 <sup>a</sup> School of Environmental and Biological Engineering, <sup>b</sup> School of Mechanical Engineering,  
9 and <sup>c</sup> School of Chemistry and Chemical Engineering, Nanjing University of Science and  
10 Technology, Nanjing 210094, China.

11  
12 <sup>‡</sup> These two authors contributed equally to this work.

13 \* Corresponding authors: lyzhu@njust.edu.cn, wanying@njust.edu.cn, and  
14 sydeng@njust.edu.cn

15

# Table of Contents

<b>Instruments</b> .....	<b>3</b>
<b>Microfluidics and Epifluorescence Imaging Setup</b> .....	<b>4</b>
Fig. S1 .....	4
<b>Synthesis of Porphyrin Receptors and Characterization</b> .....	<b>5</b>
Fig. S2 .....	5
Fig. S3 .....	6
<b>Flow Rate and Time Calibrations</b> .....	<b>6</b>
Fig. S4 .....	7
<b>Referencing and Partitioning of Regions of Interest</b> .....	<b>7</b>
Fig. S5 .....	8
<b>Chemotactic Binding Titration</b> .....	<b>9</b>
<b>Chemotaxis Focusing and Defocusing/Spreading Experiments</b> .....	<b>10</b>
Fig. S6 .....	10
<b>Metric of Chemotactic Shift</b> .....	<b>11</b>
<b>Chemotactic Titration on Methylbenzene (Toluene)</b> .....	<b>13</b>
Fig. S7 .....	13
<b>Chemotactic Titrations on <i>meso</i>- and <i>ortho</i>- Halogenated Pyridines</b> .....	<b>13</b>
Fig. S8 .....	13
Fig. S9 .....	14
<b>Spectrophotometric Titration in Bulk Solutions</b> .....	<b>14</b>
Fig. S10 .....	15
Fig. S11 .....	16
Fig. S12 .....	16
<b><sup>1</sup>H Diffusion-Ordered Nuclear Magnetic Resonance (NMR) Spectroscopy</b> .....	<b>17</b>
Fig. S13 .....	19
<b>Source Code for Numerical Simulation</b> .....	<b>20</b>
Table S1 .....	23
Fig. S14. ....	23
Fig. S15. ....	24
<b>Kernel Functions</b> .....	<b>24</b>
<b>Viscosity and Reynolds Number Measurements</b> .....	<b>26</b>
Fig. S16 .....	26
<b>References</b> .....	<b>27</b>

## Materials and Reagents

*meso*-Tetrakis(4-carboxyphenyl)porphine (TCPP, C<sub>48</sub>H<sub>30</sub>N<sub>4</sub>O<sub>8</sub>, M<sub>w</sub>: 790.8) and oxalyl chloride were purchased from Frontier Scientific, Inc. (Logan, UT). *N,N*-Diisopropylethylamine, *N,N*-dimethylformamide (DMF), pyridine, methylbenzene, 2-fluoropyridine, 2-chloropyridine, 2-bromopyridine, 3-fluoropyridine, 3-chloropyridine, 3-bromopyridine, oxalyl chloride and zinc acetate (Zn(OAc)<sub>2</sub>) were ordered from Sigma-Aldrich Co. (St. Louis, MO). Di-*n*-octyl-amine and trioctylamine were procured from Alfa Aesar Chemicals (Tewksbury, MA). 3,4,5-Tris((*S*-3,7-dimethyl-octyl)oxy)aniline (TOA, C<sub>36</sub>H<sub>67</sub>NO<sub>3</sub>, M<sub>w</sub>: 561.5) was purveyed from WuXi App. Tec. CDCl<sub>3</sub> (deuterated chloroform, containing 0.03% v/v tetramethylsilicone (TMS)) and methylcyclohexane (MCH) were bought from Energy Chemical Co., Ltd. (Shanghai). Unless being otherwise specified, all chemicals were of analytical grade and used as received.

## Instruments

Field-emission environmental scanning electron microscopy (FE-ESEM) was conducted on a FEI Quanta 250 FEG microscope at 5.0 kV (Zeiss, German). 10 μL of 0.1 mM ZnTCPP-TOA with 0.5 mM and 1 M pyridine was premixed respectively, dropped onto pieces of clean silicon wafer (ultra-flat P 2", EMS), and air dried. After platinum plating (10 min Pt powder sputtering under vacuum, Quorum Technologies), it was placed on the sample stage for the sight of morphology. Confocal laser-scanning images across a local zone of 512×512 pixel<sup>2</sup> were shot on a super-resolution system (Nikon, Japan) that comprises modules of Ti2-E Confocal, A1 Total internal reflection fluorescence (TIRF), plus Structured illumination microscopy (SIM). Again, 10 μL of each foregoing sample was pipetted on a glass slide (50 mm×22 mm×0.15 mm, Fisherbrand) and capped with a coverslip (30 mm×10 mm×1 mm, Fisherbrand) prior to the microscopic examination in NIS-Elements Viewer v5.21 in an 63X objective (Plan, Apo λ, ∞/0.17, N.A. 1.40 oil, W.D. 0.13) through 535-nm filter (rendered in green hue) under 10 s exposure at 1~2 frame per second.

All pieces of glass had been cleaned in a near-boiling mixture (1:7 v/v) of 7X detergent (MP Biomedicals, LLC., Solon, OH) and ultrapure water (≥18.2 MΩ·cm, from an EPED Plus-E3 TS Purification System, Nanjing) for 2 h on ceramic stands, and rinsed thoroughly with double-distilled H<sub>2</sub>O and blown dry with N<sub>2</sub>. The pretreated glasses got annealed in a muffle furnace at 530 °C for 6 h.

## Microfluidics and Epifluorescence Imaging Setup

A 3-inlet  $\Psi$ -shaped microfluidic channel with a dimension of 18.5 mm in full length (inlets and outlet precluded), 284  $\mu\text{m}$  in inner width and 100  $\mu\text{m}$  in height was custom-designed and made out of anti-swelling soda lime glass by wet-etching for this study. For microfluidic experimentation (Fig. S1), three glassy injectors (Shanghai bio., 1 mL, inner diameter: 45 mm) were paralleled on a LSP04-1A syringe pump (Langer, Baoding), and wired to the microchip through stainless steel needles ( $\Phi$  0.71 mm $\times$ 25 mm) plus TFT20024 Natural Teflon tubings (thin wall,  $\Phi$  0.51 mm, Alpha-Wire).

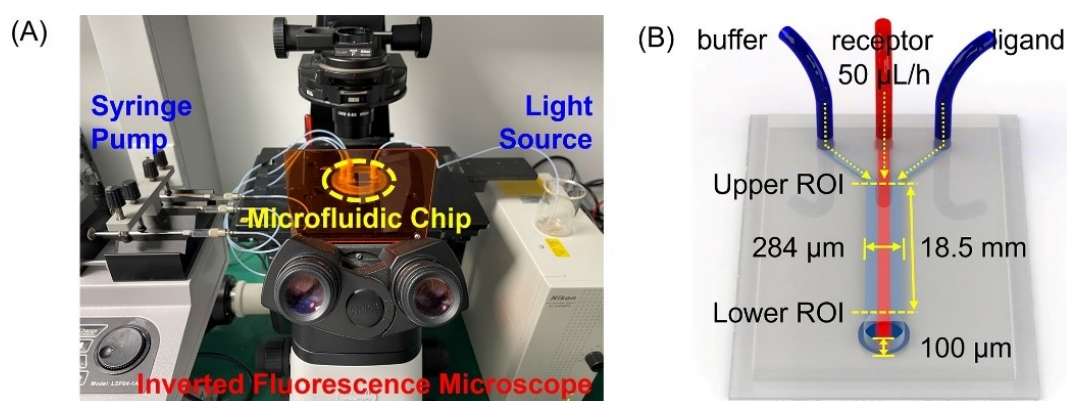


**Fig. S1** (A) Photograph of the microfluidic observation platform. (B) Schematic illustration of a 3-inlet microfluidic channel for chemotaxis studies.

The collective migration of the compound ZnTCPP-TOA in response to the ligand gradients was visualized using a Ti2-U inverted epifluorescence microscope (Nikon, Japan). The incident light beam out of a green filter ( $\lambda_{\text{ex}} = 538\sim 580$  nm) was focused onto the device bottom via a 20X objective (Plan, Ph1 DL  $\infty/-$ , N.A. 0.25, W.D. 10.5). The cross-channel photoluminescent (PL) pictures were captured by a DS-Qi2 sCMOS monochrome camera over 20-min timelapse at an interval of 30 s in NIS-Elements AR software (Exposure: 1 s). Averaged over at least three independent repeats, the mean PL intensities after background removal were plotted as a function of channel width at designated regions of interest (ROI), and further normalized with Origin 8.0 software (OriginLab Corporation).

## Synthesis of Porphyrin Receptors and Characterization

TOA-appended ZnTCPP (ZnTCPP-TOA) was prepared following a modified 3-step process reported by Helmich *et al.*<sup>[S1]</sup> as illustrated in Fig. S2.

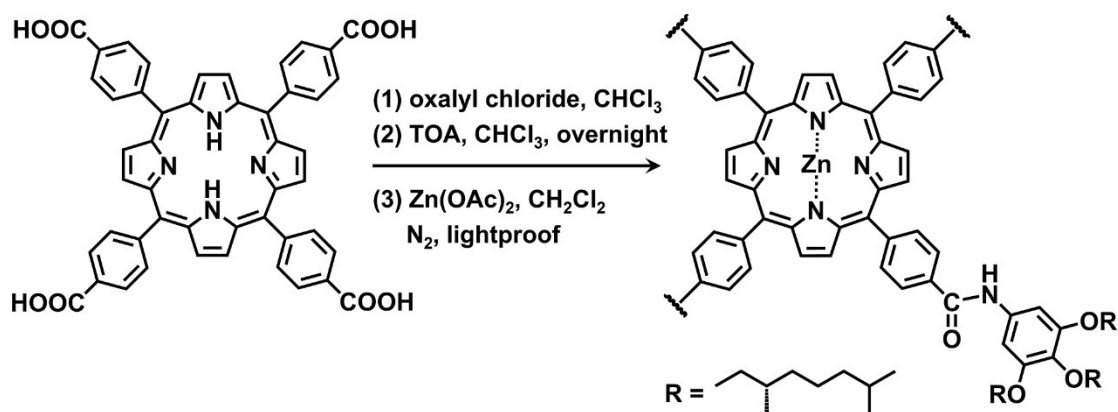


**Fig. S2** A simplistic synthesis route of ZnTCRP-TOA.

(1) TCPP (135 mg,  $1.71 \times 10^{-4}$  mol) was suspended in 15 mL of  $\text{CHCl}_3$  in a flamed flask, where 350  $\mu\text{L}$  of oxalyl chloride ( $4.14 \times 10^{-3}$  mol) was added after stirring stabilized along with two drops of dehydrated DMF. The lightproof reactor was agitated overnight in the atmosphere of nitrogen, then desolventized dry with  $\text{N}_2$  blasts. Residual volatiles were further vaporized in a vacuum oven at 65  $^\circ\text{C}$  for 2 h to obtain the acyl chlorinated TCPP (TCPP-Cl).

(2) TCPP-Cl was redissolved in 8.5 mL chloroform containing TOA (769 mg,  $1.37 \times 10^{-3}$  mol) and *N,N*-diisopropylethylamine (700  $\mu\text{L}$ ,  $4.02 \times 10^{-3}$  mol) and subjected to 48-h stirring in dark under  $\text{N}_2$  protection, whereafter 60 mL of  $\text{CHCl}_3$  was introduced to dilute the mixture followed by sequential extraction against 10 wt.% aqueous citric acid (10 mL $\times$ 3 times), 1 M NaOH (10 mL $\times$ 2), and brine (10 mL $\times$ 1). The organic phase was separated out, desiccated with anhydrous  $\text{Na}_2\text{SO}_4$ , and suction filtered. The crude product was purified via column chromatography of silica gel, eluting with 3:1 heptane/ethyl acetate to yield a purple solid, *i.e.* TCPP-TOA.

(3) TCPP-TOA was redispersed in dichloromethane ( $\text{CH}_2\text{Cl}_2$ ), and excess  $\text{Zn}(\text{OAc})_2$  (500 mg,  $2.73 \times 10^{-3}$  mol) was supplemented under agitation in shade overnight. The blend underwent film filtration, rotary evaporation, and again chromatographic purification with 4:4:1 heptane/ $\text{CHCl}_3$ /ethyl acetate as a developing agent to obtain the final purplish red crystallites in 78% productivity (403 mg), referred to as ZnTCPP-TOA.

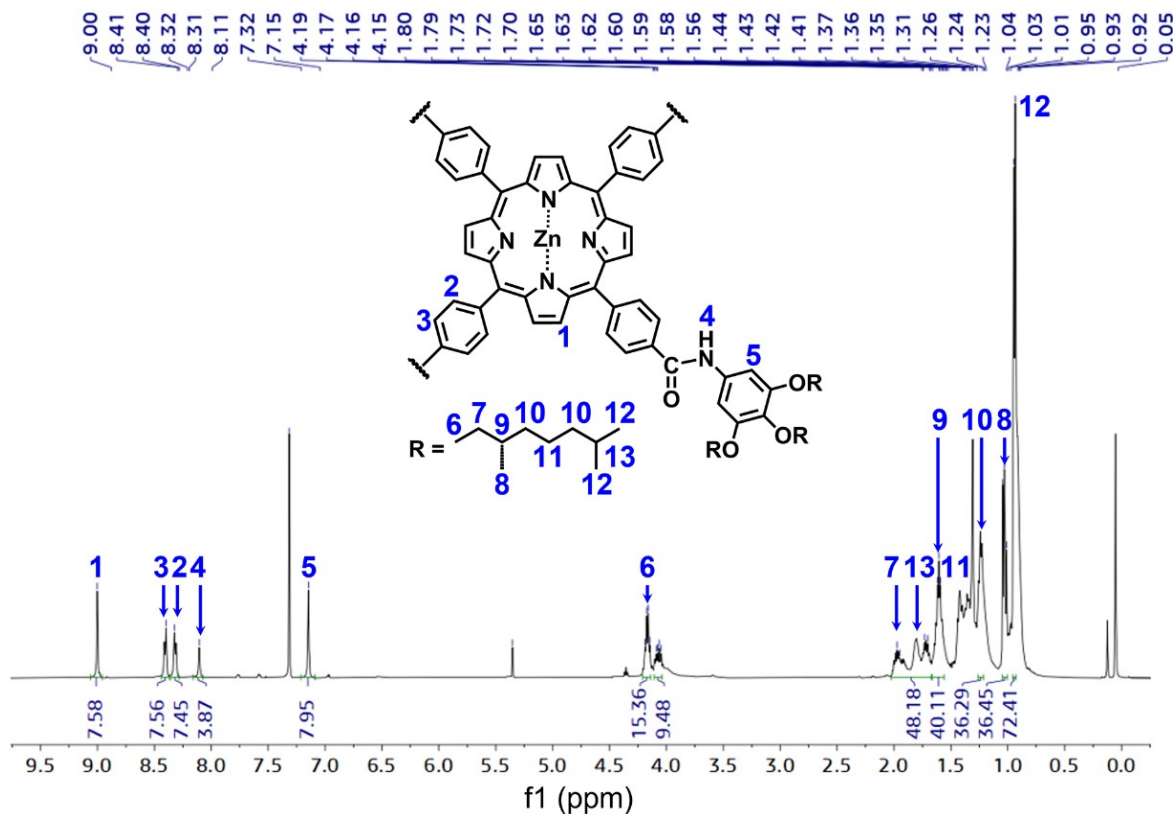


**Fig. S3**  $^1\text{H-NMR}$  spectral characterization of ZnTCPP-TOA and its inset structure with the assignments of hydrogens in alphabet. The peak integral ratio of chemical shifts ( $\delta$ ) at 9.00 (*s*, 8H), 8.41/8.42 (*d*, 8H), 8.32/8.31 (*d*, 8H), and 7.15 (*s*, 8H) is 1:1:1:1 that ascribed to the characteristic H on the porphine ring; whereas a new H-shift appears at 8.11 (*s*, 4H) with a half intensity integration, indicating the successful amidation between TOA and TCPP.

## Flow Rate and Time Calibrations

In the 20X objective, the unit size of 1 pixel corresponds to  $0.42\ \mu\text{m}$  at the magnification factor = 1. In this way, the width of the microfluidic main body was calculated to be  $284\ \mu\text{m}$  ( $884 - 204 = 180$  pixels). Other geometries are the channel height:  $100\ \mu\text{m}$ , the cross-sectional area:  $2.84 \times 10^{-2}\ \mu\text{m}^2$ , the width of inlet lanes:  $100\ \mu\text{m}$ , and their branching angle:  $45^\circ$ .

Excluding the radii of punctured holes, the length from conflux to outlet was measured to be  $18.5\ \text{mm}$ . Since the volumetric speed imposed by the constant pressure pump was chosen to be  $50\ \mu\text{L} \cdot \text{h}^{-1}$  (this optimum is validated in Fig. S4) upon all three inlets and the  $\Phi$  of syringes in use was gauged  $4.5\ \text{mm}$  by a vernier caliper, the mean linear velocity was estimated to be  $2.3\ \text{mm} \cdot \text{s}^{-1}$ . Theoretically, it would take  $10.3\ \text{s}$  for fluids running over the whole channel.

The accurate passing time was further calibrated in practice with the fluorescent dye-tagged microsphere. By monitoring the displacement of targeted fluorescent microspheres ( $5.0\ \mu\text{m}$ ,

Aladdin, Inc., 0.1 mg/mL) down the center of main channel among consecutive video (Frame: 20 ms), a calibrated flow time was updated to be 11.2 s. This length and the timescale are sufficient to deliver observable diffusion and reaction progress near the outlet.

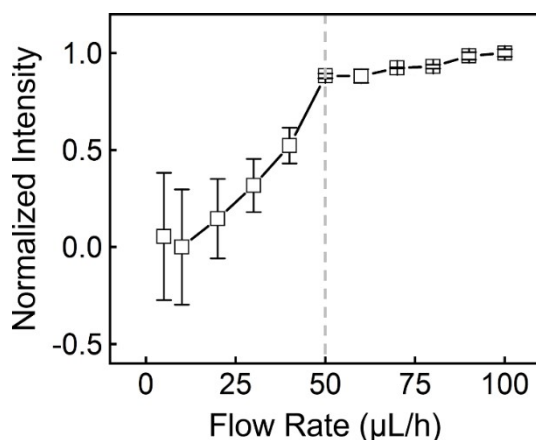


**Fig. S4** Dependence of the stability in dye signals upon the flow rate.

### Referencing and Partitioning of Regions of Interest

For precise positioning during back-and-forth stage moves and refocusing, a set of reference lines were drawn that marked in endpoint coordinates as  $(x_1, y_1) \rightarrow (x_2, y_2)$  to align the micro-channel. Typical segments in the Showlive window ( $1022 \times 1022$  pixel<sup>2</sup>, binning: 1) are denoted as follows:

1. Crosswire:  $x$ -axis  $(0, 544) \rightarrow (1636, 544)$ ,  $y$ -axis  $(818, 0) \rightarrow (818, 1088)$ ;
2. Channel innerwalls: left edge  $(560, 204) \rightarrow (1636, 204)$ , right edge  $(560, 884) \rightarrow (1636, 884)$ , left inlet  $(0, 0) \rightarrow (560, 204)$ , right inlet  $(0, 1088) \rightarrow (560, 884)$ ;
3. Vertical trifurcation:  $(818, 0) \rightarrow (818, 544)$ ,  $(0, 544) \rightarrow (818, 544)$ ;
4. Confluence:  $(560, 204) \rightarrow (560, 884)$ .

To minimize background signals out of the weak internal reflection at the coverslip surface, the sampling linescan always spanned 10-pixel wider than the channel width in display (*i.e.* 5 pixels away from each side). In terms of proper magnification, the channel was divided from entry to exit into two major parts along the flow. Namely, the upper ROI that includes all three inlets pointing straight towards upper left and right angles of the observation window; whereas the landmark - an inconspicuous spot at  $(1000, 200)$  defines the lower ROI. The PL emission profile as a function of lateral distance were constantly sampled at:

1. Confluence in the upper ROI to check whether the initial status kept the same among different inflow configurations (Fig. S5D);
2. (1000, 204)  $\rightarrow$  (1000, 884) in the lower ROI to record the collective migration of receptors in the middle lane at their most diffusiveness. (Fig. S5E).

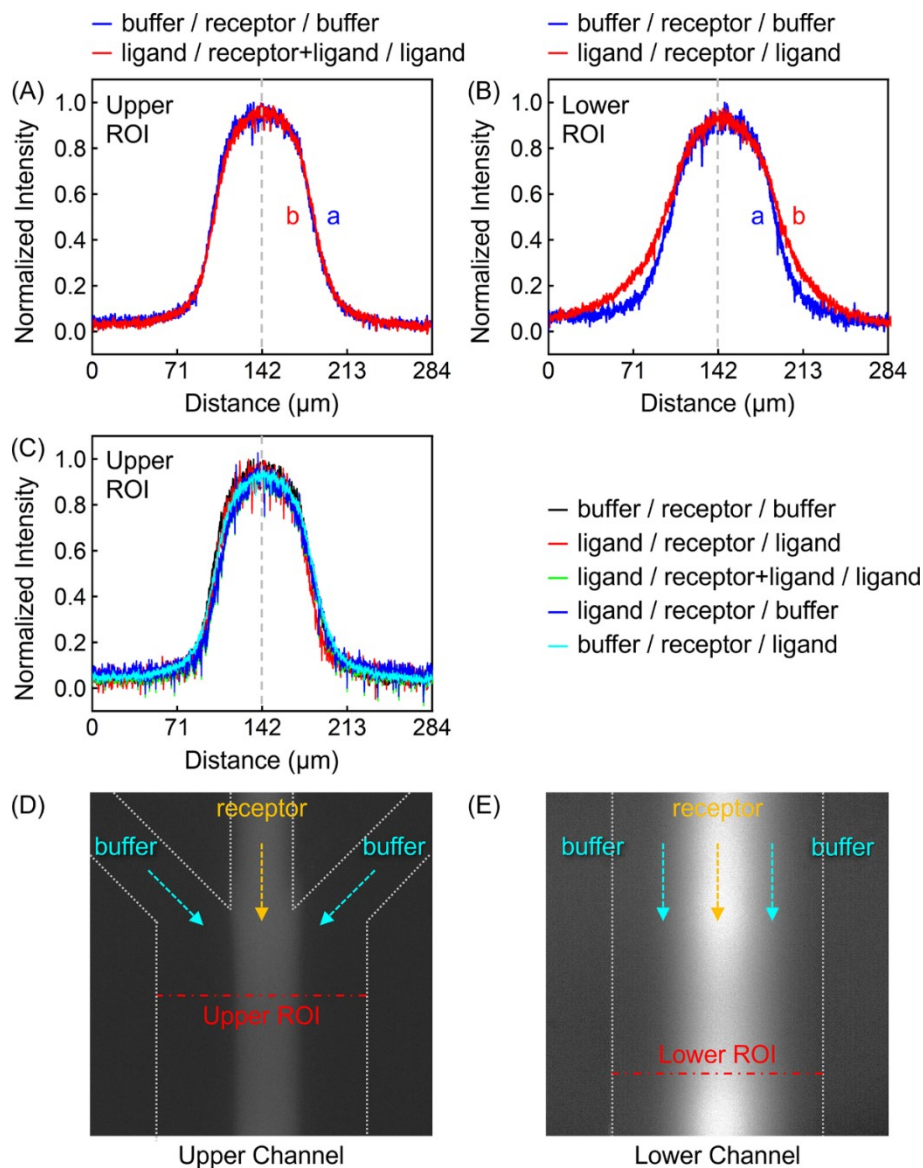


**Fig. S5** Normalized intensity profiles at upper ROI of 100  $\mu\text{M}$  ZnTCPP-TOA (receptor) in the center and 100 mM pyridine (ligand) in (A) all three lanes and (B) the right lane. The red line corresponds to ligand-present situation, while blue the ligand-absent. (C) Merged profiles at upper ROI involving five different regimes. (D)(E) Typical snapshots on steady flow at appointed upper and lower ROI, respectively. The dashed segments encompass the channel outline, and the dash-dotted highlights the sampling position.

## Chemotactic Binding Titration

The binding strengths of ZnTCPP-TOA the receptor with a handful of *N*-ligands were inspected via an overall protocol showcased below:

(1) Three syringes were loaded in a row on the pump rack and pushed in the same pace to infuse slowly and steadily through Teflon tubings. All consumables were disposed per run.

(2) To begin with, all conduits were rinsed with MCH at  $200 \mu\text{L}\cdot\text{min}^{-1}$  for a total of 0.35 mL to wet entire pipeline. Owing to weak surface tension in organic solvents, debubbling was taken quite easy without the bother of any deliberate actions.

(3) MCH containing either  $100 \mu\text{M}$  ZnTCPP-TOA or certain *N*-ligand, *e.g.* pyridine at specific content was docked separately onto one of the three inlets in an order from left to right as MCH/ ZnTCPP-TOA/pyridine, and conducted to a waste recipient from outlet. The fluidic patterns at upper and lower ROIs were tracked over time by periodical exposures. 20 minutes of relaxation were required before access to a interdiffusion balance.

(4) The lateral distribution in terms of PL intensity of ZnTCPP-TOA was used to indicate its concentration gradient. Its profile was compared with the basic set (the blank control) of MCH/ ZnTCPP-TOA/MCH and the discrepancy between, *i.e.* the chemotactic shift, was quantified and compiled for binding assays.

## Chemotaxis Focusing and Defocusing/Spreading Experiments

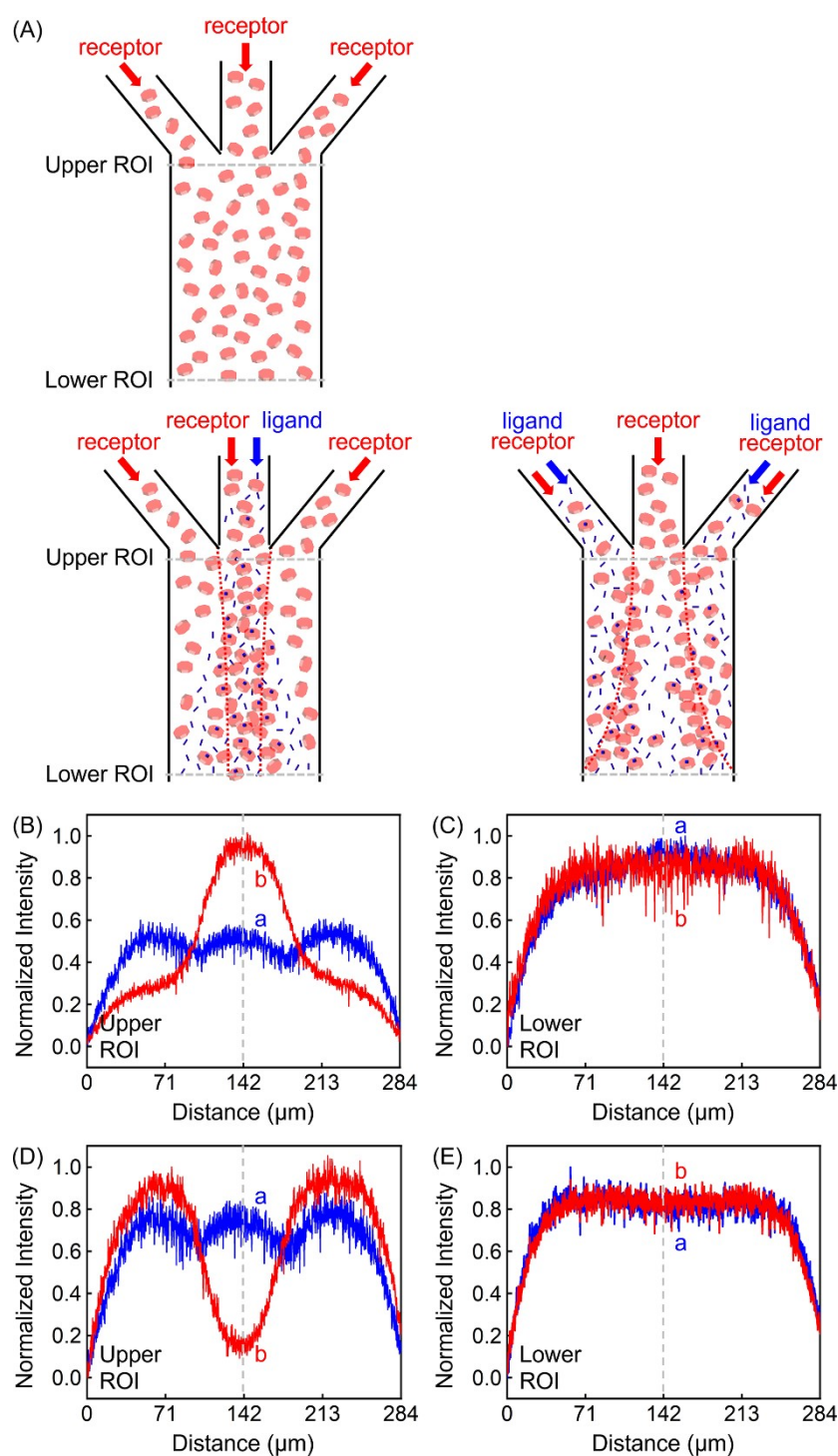


**Fig. S6** Upper panel: Illustrated channel inflows and diffusion status of (A) the basic set or the blank control as receptor/receptor/receptor in MCH (1<sup>st</sup> row), and (B) the inverted focusing/spreading regimes as receptor/receptor+ligand/receptor (2<sup>nd</sup> row on the left) and receptor+ligand/receptor/receptor+ligand (2<sup>nd</sup> row right). Lower panel: Normalized intensity distribution at (B) Upper and (C) Lower ROI of 100  $\mu\text{M}$  ZnTCPP-TOA in full channel (blue) vs. 100  $\mu\text{M}$  ZnTCPP-TOA+100 mM pyridine in the middle flanked by 100  $\mu\text{M}$  ZnTCPP-TOA in side channels (red); (D) Upper and (E) Lower ROI of 100  $\mu\text{M}$  ZnTCPP-TOA in full channel (blue) vs. 100  $\mu\text{M}$  ZnTCPP-TOA + 100 mM pyridine in side channels while 100  $\mu\text{M}$  ZnTCPP-TOA in the middle (red).

## Metric of Chemotactic Shift

Assuming the receptor-ligand binding system as an ensemble index  $\alpha$ , the solutions flow down in  $z$  direction and the lateral position is defined by  $x$ , which specifies the distance from the channel wall in a range of  $0 \leq x \leq L$ , where  $L$  is the channel width. The PL intensity,  $\hat{\gamma}_\alpha(x)$ , is observable as a function of  $x$  over a slab of  $dz$  along the channel axle, while its minimum is expressed as:

$$\hat{\gamma}_{\alpha|min} = \min_{x \in [0, L]} \hat{\gamma}_\alpha(x) \quad (\text{S1})$$

Hence, the normalized  $\hat{\gamma}_\alpha(x)$ ,  $I_\alpha(x)$ , can be derived as:

$$I_\alpha(x) = \frac{\hat{\gamma}_\alpha(x) - \hat{\gamma}_{\alpha|min}}{\hat{N}_\alpha} \quad (\text{S2})$$

in which

$$\hat{N}_\alpha = \int_0^L dx [\hat{\gamma}_\alpha(x) - \hat{\gamma}_{\alpha|min}] \quad (\text{S3})$$

The denominator as Eq. S4 makes Eq. S3 significant in both physics (mass conservation) and statistics (definitive and comparable), whereby  $I_\alpha$  can be treated as a probability distribution with a reciprocal length unit. In particular,  $I_\alpha(x)$  is directly associated with the number density of receptors, which further gives rise to two following premises:

1. The measured  $\hat{\gamma}_\alpha(x)$  is linearly related to the receptor density according to

$$\hat{\gamma}_\alpha(x) = k_\alpha \rho_\alpha(x) + b_\alpha \quad (\text{S4})$$

Here,  $k_\alpha$ ,  $\rho_\alpha(x)$  and  $b_\alpha$  represents the contributor of each dye, the number density at  $x$ , and the background noise, respectively. Note that  $k_\alpha$  and  $b_\alpha$  are  $x$ -independent yet may vary from one condition to the other.

2.  $\hat{\gamma}_{\alpha|min}$  provides a good estimate of  $b_\alpha$ :

$$\hat{\gamma}_{\alpha|min} \approx b_\alpha \quad (\text{S5})$$

or equivalently,

$$\rho_{\alpha|min} - b_{\alpha} = \frac{\hat{\gamma}_{\alpha|min} - b_{\alpha}}{k_{\alpha}} \approx 0 \quad (\text{S6})$$

If both satisfied, then  $\hat{\gamma}_{\alpha}(x) - \hat{\gamma}_{\alpha|min} = k_{\alpha}\rho_{\alpha}(x)$  and  $\hat{N}_{\alpha} = k_{\alpha}N_{\alpha}$ , where

$$N_{\alpha} = \int_0^L dx \rho_{\alpha}(x) \quad (\text{S7})$$

is the total number of receptors contributing to the PL emission in  $dz$  at  $z$ . Moreover,

$$\hat{\gamma}_{\alpha}(x) = \frac{\rho_{\alpha}(x)}{N_{\alpha}} \quad (\text{S8})$$

such that  $I_{\alpha}(x)dx$  is the fraction of receptors in  $dx$  at  $x$ .

In this sense, one can quantify the chemotaxis of receptors in terms of  $I_{\alpha}(x)$  as:

$$\mu_{\alpha} = \int_0^L dx I_{\alpha}(x)x \quad (\text{S9})$$

where  $\mu$  is the first moment or cumulant, signifying the most expectant position of receptors at given  $\alpha$ . Furthermore,

$$\sigma_{\alpha}^2 = \int_0^L dx I_{\alpha}(x)(x - \mu_{\alpha})^2 = \int_0^L dx I_{\alpha}(x)x^2 - \mu_{\alpha}^2 \quad (\text{S10})$$

is the second cumulant (the variance). Its root,  $\sigma_{\alpha}$ , is the standard deviation.

The chemotactic shift is thus measurable based on the subtraction of  $I_{\alpha}(x)$  in presence of ligands (*i.e.*  $\alpha = L$ ) from the absence regime (*i.e.* the control,  $\alpha = C$ ):

$$\delta\mu = \mu_L - \mu_C = \int_0^L dx [I_L(x) - I_C(x)]x \quad (\text{S11})$$

Note that  $\delta\mu < 0$  when the displacement goes left (*e.g.* pyridine/ZnTCRP-TOA/MCH). In this case, the absolute  $\delta\mu$ ,  $|\delta\mu|$ , would make the algorithm port-invariant in the collective migration activity. On the other hand, to handle the receptor spreading/focusing scenario with  $\delta\mu = 0$ , an alternative solution is:

$$\delta\sigma = \sigma_L - \sigma_C = \sqrt{\int_0^L dx I_L(x)(x - \mu_L)^2} - \sqrt{\int_0^L dx I_C(x)(x - \mu_C)^2} \quad (\text{S12})$$

## Chemotactic Titration on Methylbenzene (Toluene)

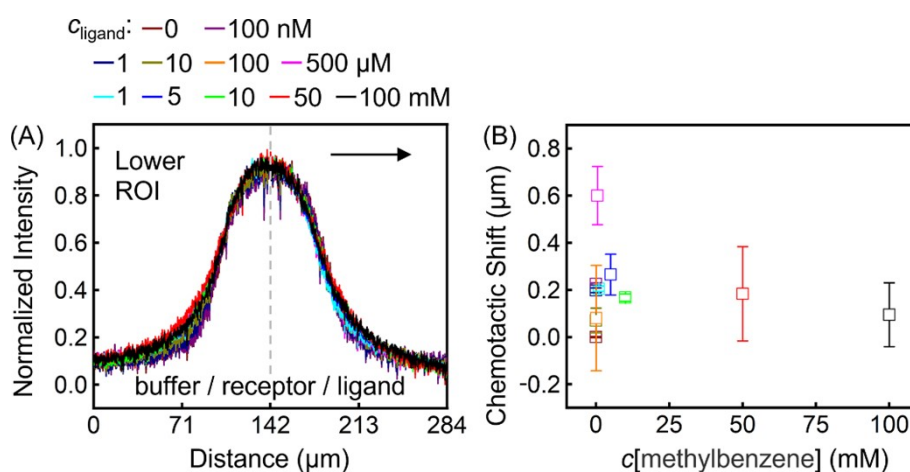


**Fig. S7** (A) Normalized intensity profiles at lower ROI of 100  $\mu\text{M}$  ZnTCPP-TOA in presence of methylbenzene. The inset arrow directs the shifting propensity with increasing amounts of ligands from 0 to 100 mM. (B) The peak displacements for toluene.

## Chemotactic Titrations on *meso*- and *ortho*- Halogenated Pyridines

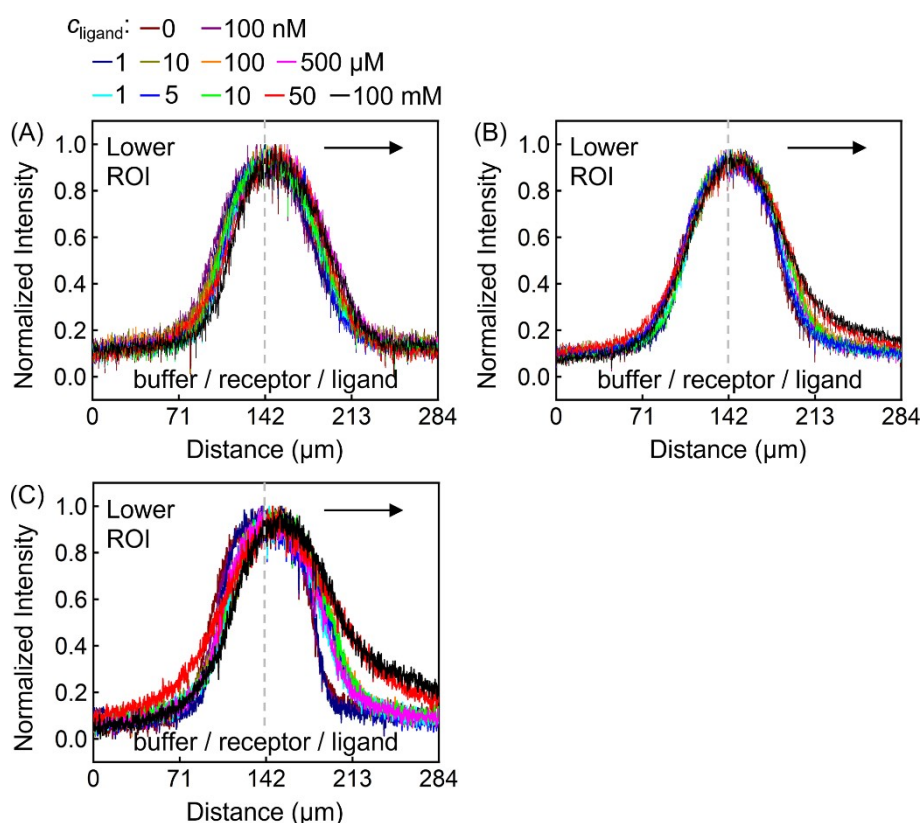


**Fig. S8** Normalized intensity profiles at lower ROI of 100  $\mu\text{M}$  ZnTCPP-TOA in presence of three kinds of 3-substituted pyridyl homologues: (A) 3-fluoropyridine (3-PyF), (B) 3-chloropyridine (3-PyCl), and (C) 3-bromopyridine (3-PyBr). The inset arrow directs the shifting propensity with increasing amounts of ligands from 0 to 100 mM.

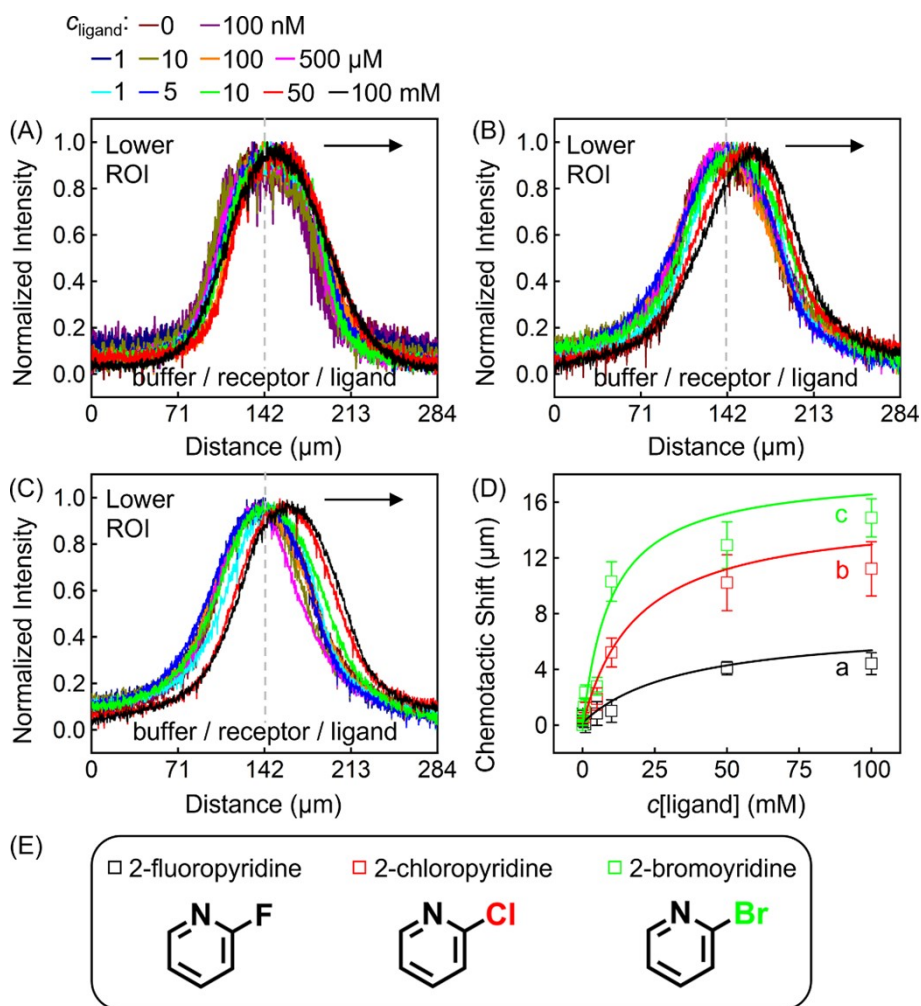


**Fig. S9** Normalized PL intensity profiles for 100 μM ZnTCPP-TOA in the presence of varying concentrations of (A) 2-fluoropyridine (2-PyF), (B) 2-chloropyridine (2-PyCl), (C) 2-bromopyridine (2-PyBr). The arrow specifies the leftward trend of profiles with increasing ligand concentrations. (D) The peak displacements for the three as 2-PyF (a), 2-PyCl (b), and 2-PyBr (c). The solid lines stand as the best fits to Eq. (1). (E) Molecular structures of each ligand.

### Spectrophotometric Titration in Bulk Solutions

Both UV-Vis and PL spectrophotometries were performed on a SpectraMax M3 Multi-Mode Microplate Reader (Molecular Devices, U.S.). The dissociation constant  $K_D$  between ZnTCPP-TOA and *N*-ligands was determined over aliquoted titrants out of the sigmoidal function below:

$$\Delta A (\Delta I) = \frac{B_{max} \cdot c_{ligand}}{K_D + c_{ligand}} \quad (\text{S13})$$

in which  $\Delta A$  is the difference in absorbance of a receptor solution from that containing various amount of ligands, *i.e.*  $c_{ligand}$ . By fitting the relationship between  $\Delta A$  and  $c_{ligand}$  in the fashion

of Langmuir isotherm, the value of  $K_D$  can be obtained. Likewise, for spectrofluorimetry, the intensity at corresponding  $c_{ligand}$  was area-integrated and converted to  $\Delta I$ . Subsequently, Eq. S14 was also resorted to extract  $K_D$  at equilibrium<sup>[S2]</sup>. The  $K_D$  results from this reference method were combined with those from the chemotactic titrations in [Table 1](#).

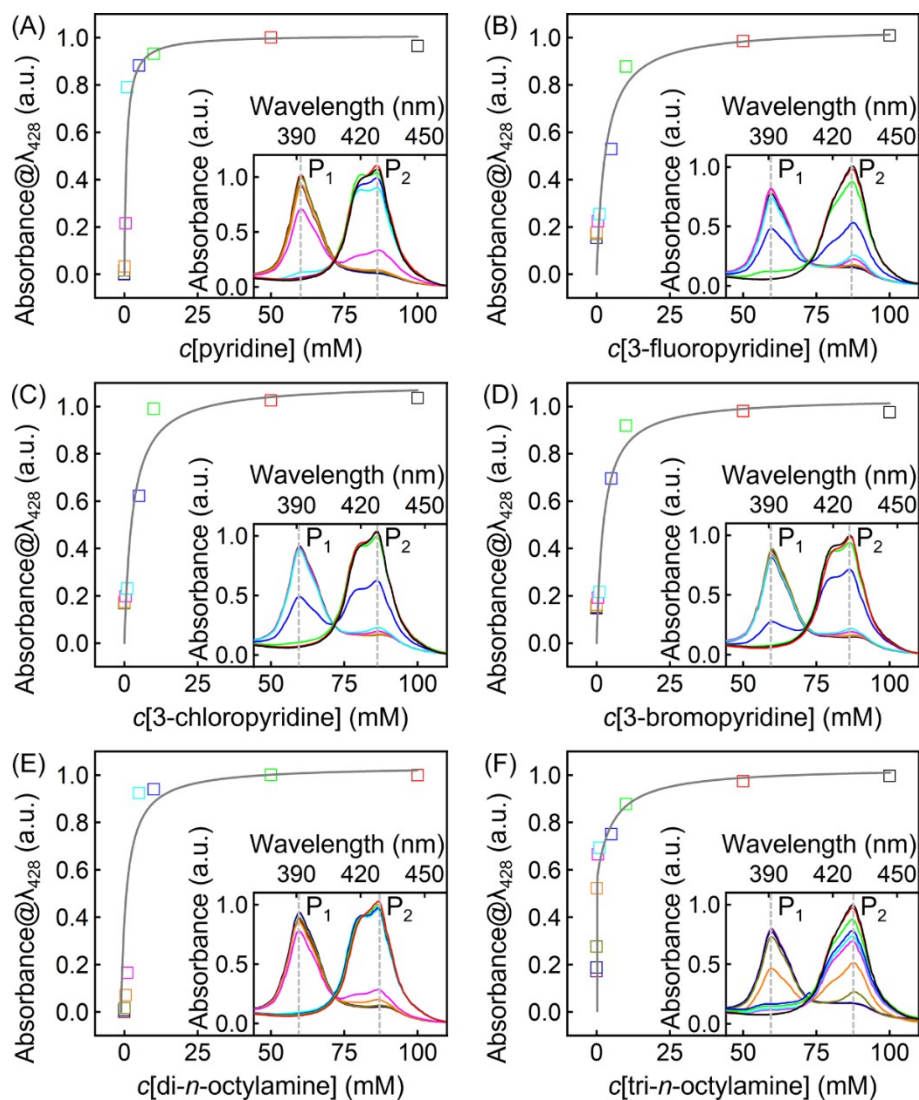


**Fig. S10** Standard curve fitted to the absorptive extremum at  $\lambda = 428$  nm in the inset. **Inset:** Absorbance titrations of ZnTCPP-TOA by UV spectrophotometry on escalating contents of (A) pyridine, (B) 3-PyF, (C) 3-PyCl, (D) 3-PyBr, (E) di-*n*-octylamine (NH(octyl)<sub>2</sub>), and (F) tri-*n*-octylamine (NH(octyl)<sub>3</sub>), where the gray-dashed line (P<sub>1</sub>) and (P<sub>2</sub>) represent characteristic peaks at 391 and 428 nm, respectively.

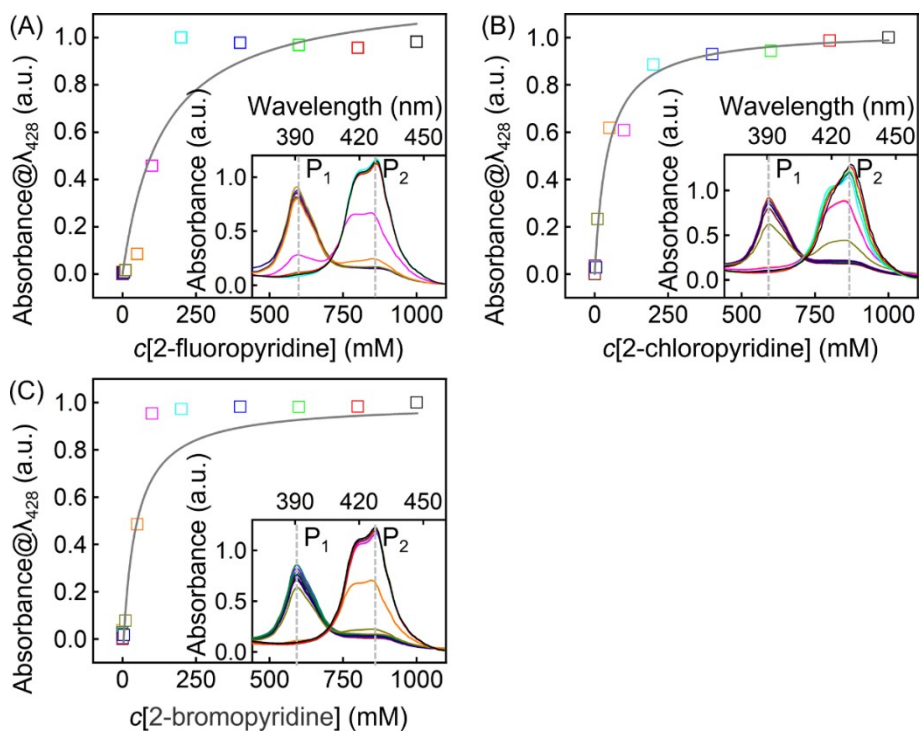


**Fig. S11** Standard curve fitted to the absorptive extremum at  $\lambda = 428$  nm in the inset. **Inset:** Absorbance titrations of ZnTCPP-TOA by UV spectrophotometry on escalating contents of (A) 2-PyF, (B) 2-PyCl, (C) 2-PyBr, where the gray-dashed line (P<sub>1</sub>) and (P<sub>2</sub>) represent characteristic peaks at 391 and 428 nm, respectively.

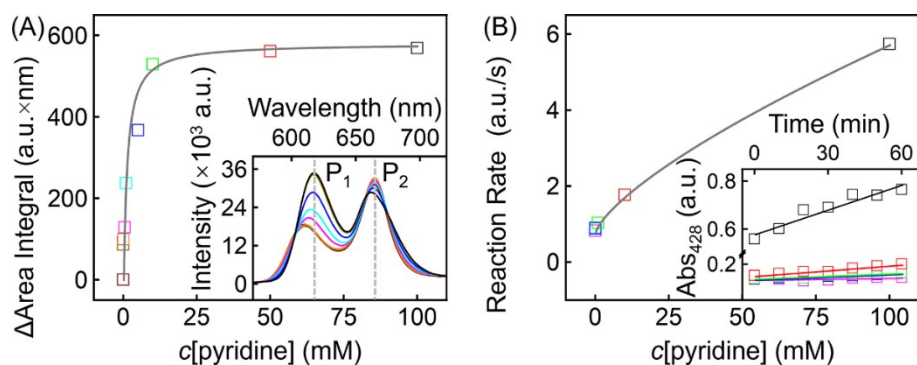


**Fig. S12** (A) Standard curve fitting the integrated area of the inset fluorescence intensity peak to the pyridine concentration. **Inset:** The spectrum measured by the fluorescence titration method, in which the grey-dashed line (P<sub>1</sub>) and (P<sub>2</sub>) represent the characteristic peaks at  $\lambda_{p1} = 616$  nm and  $\lambda_{p2} = 660$  nm, respectively; and the direction of the arrow is the change of intensity with concentration. (B) ultraviolet kinetic spectra of ZnTCPP-TOA receptors and pyridine prepared from low to high multiples (the inset is the change trend of absorbance measured with different concentrations of pyridine over time).

## **<sup>1</sup>H Diffusion-Ordered Nuclear Magnetic Resonance (NMR) Spectroscopy**

Equimolar ZnTCRP-TOA and pyridine at 1 mM were co-dissolved in deuterated MCH (MCD, 99.9%, Merck & Co.). Mere ZnTCRP-TOA was the control. 500  $\mu$ L Solution was loaded in a 5-mm high-pressure NMR tubes and sealed tight with a screw-top cap. Both 1D <sup>1</sup>H-NMR and diffusion ordered spectra (NMR-DOSY) were collected over a period of 2 h on a Bruker AV-III-HD spectrometer (500.2 MHz, 298 K) equipped with a cryo-probe (5 mm CRP BBO 500S1 BB-H&F-D-05Z, liquid N<sub>2</sub> as coolant). Data outputs were processed with MestReNova. To secure authentic signal integrals, a 4<sup>th</sup>-order polynomial was called for their baseline corrections.

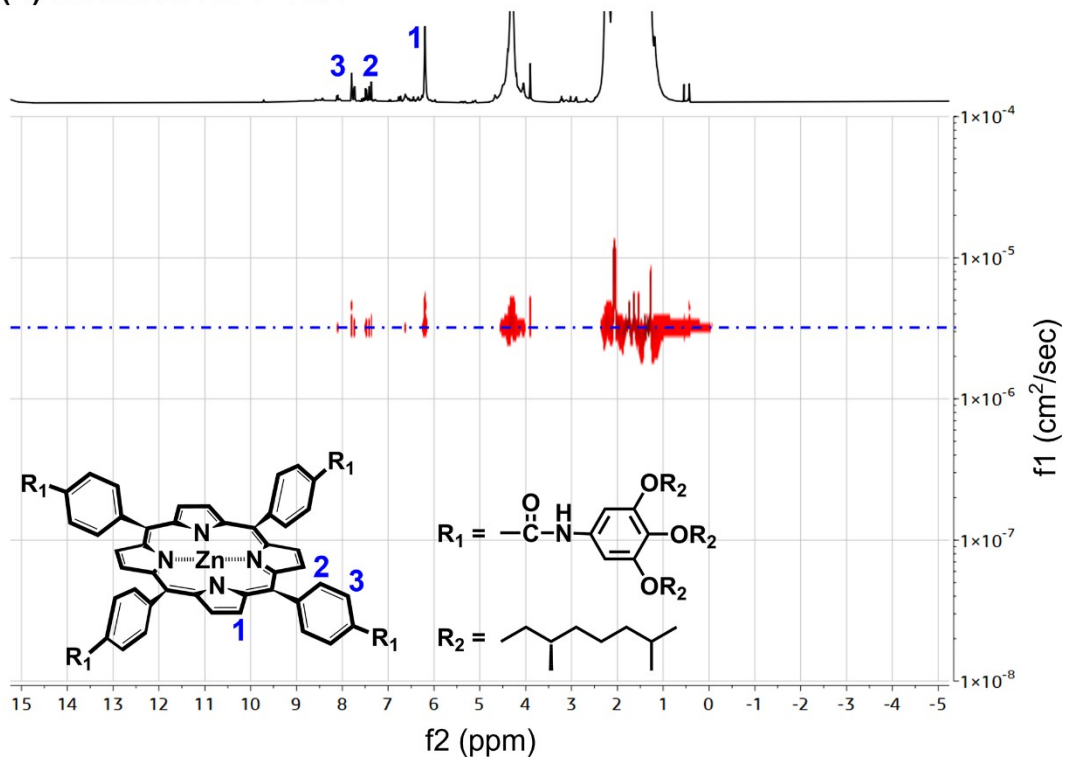
In a static magnetic field, an escalating pulsed array of radio frequencies can phase-encode nuclear spins according to molecular positions. By a diffusion delay of  $\Delta t$ , a decoding gradient of pulses is applied for an extra period ( $\delta$ ), that will not undoes the phases of molecules afar instead attenuate their resonant intensities  $I$  at a rate proportional to the diffusivity ( $D$ ) and the amplitude ( $G$ ) as formulated in Eq. S2:<sup>[S3]</sup>

$$I = I_0 \cdot \exp\left[-D(G\delta\gamma)^2\left(\Delta t - \frac{\delta}{3}\right)\right] \quad (\text{S14})$$

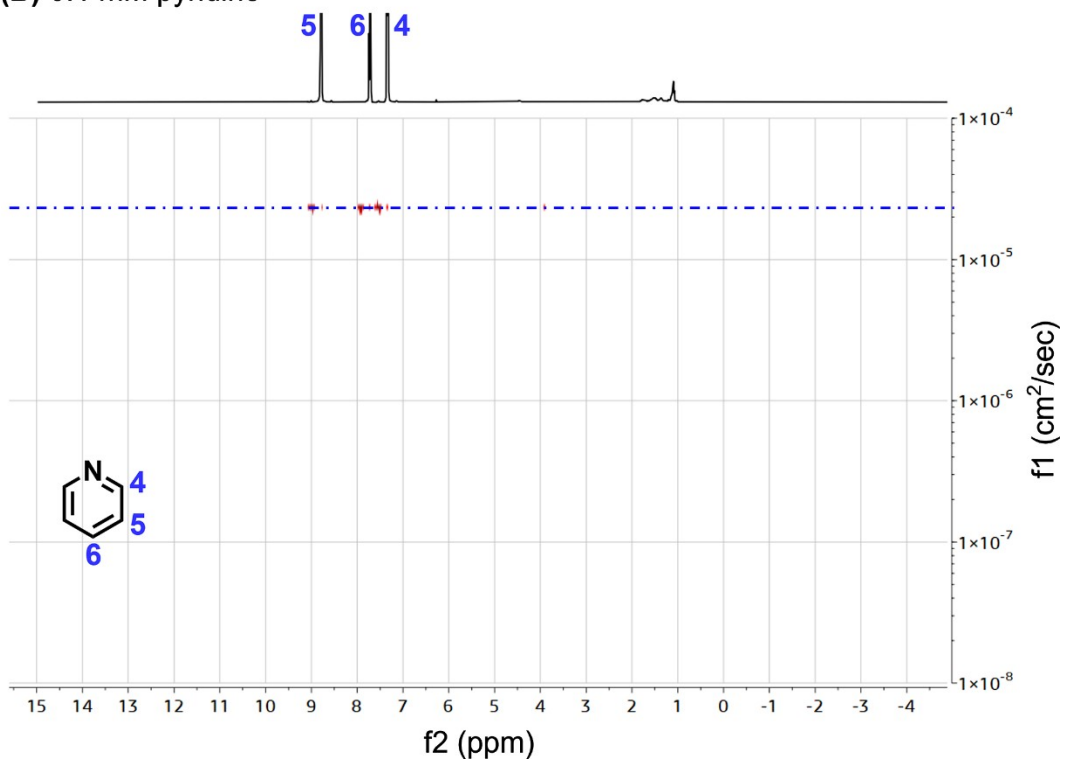
Here,  $I_0$  is the signal intensity in the absence of pulse gradient and  $\gamma$  is the magnetogyric ratio of the nucleus in interest.

In this work, a well-configured group of parameters for NMR-DOSY characterization starts with the appropriate pulse sequence of a longitudinal eddy current delay, one pair of bipolar gradient, and two spoil gradients, *i.e.* PULPROG = ledbpgp2s(1d). Other initializing inputs involve:  $\Delta t$ (D20) = 0.2 s,  $\delta$ (P30) = 1800  $\mu$ s, 16 slices, Time domain size (TD) = 16 K, Sweep width (SWH) = 3.46 ppm, Acquisition time (AQ) = 4.73 s, Center of spectrum (O1) = 7.83 ppm, Number of dummy scan (DS) = 4, Number of scan (NS) = 32, Relaxation delay (D1) = 1 s, Gradient recovery time (D16) = 0.0002 s, Spoil gradient pulse (P19) = 600 s. The pulse gradients (GPZ6[%]) ramp up linearly from 2 to 95% of its maximal strength (0.50 T·m<sup>-1</sup>) in  $z$ -axis, while the  $\Delta t$ -dependent  $\delta$  is fixed at 2% residue of the former signal.  $\Delta t$ (D21) = 5 ms for eddy current reduction. To circumvent any magnetocaloric effect, the temperature was kept down via ventilation at 350 L·h<sup>-1</sup> yet with no rotation of NMR tubes in case of artefacts like 1<sup>st</sup>-order side bands or even higher.<sup>[S4]</sup>

(A) 0.1 mM ZnTCPP-TOA



(B) 0.1 mM pyridine





## Source Code for Numerical Simulation

The program was developed with PyCharm 2019 Professional in the language of Python 3.8, that passed the benchmark tests in Windows 10 O.S.

```
import pandas as pd
import numpy as np
import csv
MAXPHI, MAXD1L, MAXD2, MAXD1R, KPMAX1, KPMAX2=
0.0, 0.0, 0.0, 0.0, 0.0, 0.0
print(
    "Enter the parameters for simulation\nInput
    numbers can be in decimal or
    scientific\nnotation, e.g., "
    "1.002 or 3.5E-9\nReaction is R + L <--> RL,
    kb/kf = KD")
LW = float(input('Enter the width of the three-
channel device in cm\n'))
TF = float(input('Enter the total time of the
simulation in seconds\n'))
CRSTAR = float(input('Enter the conc. (mol/L)
of the probe molecule in the central
channel\n'))
CLSTAR = float(input('Enter the ligand conc.
(mol/L) in the side channel\n'))
KD = float(input('Enter Kd, the dissociation
constant in M\n'))
DR = float(input('Enter the diff. const. of the
probe molecule in cm2/s\n'))
DL = float(input('Enter the diffusion constant
of the ligand in cm2/s\n'))
DRL = float(input('Enter the diff. const. of
the complex in cm2/s\n'))
# Calculate the dissociation rate constant
DMAX = 0.0
if DR > DMAX:
    DMAX = DR
if DL > DMAX:
    DMAX = DL
if DRL > DMAX:
    DMAX = DRL
MAXCD = 0.0
MAXDIFF = 0.0
# 1-D simulation in 999 diffusion boxes
L = 999
# Calculate the box width DX
DX = LW / float(L)
# Calculate the time increment for
discretization
DT = 0.45 * DX * DX / DMAX
# Calculate total number of time points
NT = int(TF / DT)
# Calculate association constant as inverse of
Kd
KA = 1 / KD
CROLD = np.arange(10001, dtype=np.float64)
CRNEW = np.arange(10001, dtype=np.float64)
CLOLD = np.arange(10001, dtype=np.float64)
CLNEW = np.arange(10001, dtype=np.float64)
CRLOLD = np.arange(10001, dtype=np.float64)
CRLNEW = np.arange(10001, dtype=np.float64)
CRCOLD = np.arange(10001, dtype=np.float64)
CRCNEW = np.arange(10001, dtype=np.float64)
# Initialize concentrations
for J in range(1, int(L / 3)+1):
    CROLD[J] = CRSTAR / 1000
    CRNEW[J] = CRSTAR / 1000
    CLOLD[J] = CLSTAR * .998
    CLNEW[J] = CLSTAR * .998
    CRLOLD[J] = CRSTAR / 1000
    CRLNEW[J] = CRSTAR / 1000
CLOLD[int(L / 3)] = CLSTAR / 2.0
CLNEW[int(L / 3)] = CLSTAR / 2.0
CROLD[int(L / 3)] = CRSTAR / 2.0
CRNEW[int(L / 3)] = CRSTAR / 2.0
for J in range(int(L / 3 + 1), int(2 * L / 3 +
1)):
    CROLD[J] = CRSTAR * .999
    CRNEW[J] = CRSTAR * .999
    CRCOLD[J] = CRSTAR * .999
    CRCNEW[J] = CRSTAR * .999
    CLOLD[J] = CLSTAR / 1000
    CLNEW[J] = CLSTAR / 1000
    CRLOLD[J] = CRSTAR / 1000
    CRLNEW[J] = CRSTAR / 1000
for J in range(int(2 * L / 3), int(L + 1)):
    CROLD[J] = CRSTAR / 1000
    CRNEW[J] = CRSTAR / 1000
    CLOLD[J] = CLSTAR / 1000
    CLNEW[J] = CLSTAR / 1000
    CRLOLD[J] = CRSTAR / 1000
```

```

CRLNEW[J] = CRSTAR / 1000

# Calculate factor df = dt/(dx)2
DF = DT / (DX * DX)
DRF = DR * DF
DLF = DL * DF
DRLF = DRL * DF

# Main iteration loop

for K in range(1, NT + 1):
    # Diffusion beyond the first box
    for J in range(2, L):
        D2R = (CROLD[J - 1] - 2 * CROLD[J] +
CROLD[J + 1])
        D1R = (CROLD[J + 1] - CROLD[J])
        D2L = (CLOLD[J - 1] - 2 * CLOLD[J] +
CLOLD[J + 1])
        D1L = (CLOLD[J + 1] - CLOLD[J])
        CRNEW[J] = CROLD[J] + DRF * D2P
        CRCNEW[J] = CRCOLD[J] + DRF * (CRCOLD[J
- 1] - 2 * CRCOLD[J] + CRCOLD[J + 1])
        CLNEW[J] = CLOLD[J] + DLF * D2L
        CRLNEW[J] = CRLOLD[J] + DRLF *
(CRLOLD[J - 1] - 2 * CRLOLD[J] + CRLOLD[J + 1])
        # Cross - diffusion beyond the first
box
        PHI = KA / (1 + KA * CLNEW[J])
        DRHI = (KA / (1 + KA * CLNEW[J + 1]) -
KA / (1 + KA * CLNEW[J]))
        CD = (PHI * (CRNEW[J] * D2L + D1R *
D1L))

# Diagnostics
if PHI > MAXPHI:
    MAXPHI = PHI
if D1R > MAXD1R:
    MAXD1R = D1R
if D1L < MAXD1L:
    MAXD1L = D1L
if D2R > MAXDIFF:
    MAXDIFF = D2P
DL2 = PHI * CRNEW[J] * D2L
if DL2 > MAXDIFF:
    MAXDL2 = DL2
if (D1L * D1R) < MAXD2:
    MAXD2 = D1L * D1R

CRNEW[J] = CRNEW[J] - DRF * PHI *
(CRNEW[J] * D2L + D1R * D1L)

```

```

CRNEW[J] = CRNEW[J] - DRF * CRNEW[J] *
DRHI * D1L

# Diffusion and cross-diffusion into the
first box
D2R = CROLD[2] - CROLD[1]
D1R = (CROLD[2] - CROLD[1])
D2L = CLOLD[2] - CLOLD[1]
D1L = (CLOLD[2] - CLOLD[1])
CRNEW[1] = CROLD[1] + DRF * D2P
CRCNEW[1] = CRCOLD[1] + DRF * (CRCOLD[2] -
CRCOLD[1])
CLNEW[1] = CLOLD[1] + DLF * D2L
CRLNEW[1] = CRLOLD[1] + DRLF * (CRLOLD[2] -
CRLOLD[1])
PHI = KA / (1 + KA * CLNEW[1])
CRNEW[1] = CRNEW[1] + DRF * PHI * (CRNEW[1]
* D2L + D1R * D1L)

# Diffusion and cross-diffusion into the
last box
D2R = CROLD[L] - CROLD[L - 1]
D1R = (CROLD[L] - CROLD[L - 1])
D2L = CLOLD[L] - CLOLD[L - 1]
D1L = (CLOLD[L] - CLOLD[L - 1])
CRNEW[L] = CROLD[L] - DRF * D2P
CRCNEW[L] = CRCOLD[L] - DRF * (CRCOLD[L] -
CRCOLD[L - 1])
CLNEW[L] = CLOLD[L] - DLF * D2L
CRLNEW[L] = CRLOLD[L] - DRLF * (CRLOLD[L] -
CRLOLD[L - 1])
PHI = KA / (1 + KA * CLNEW[L])
CRNEW[L] = CRNEW[L] - DRF * (PHI) *
(CRNEW[L] * D2L + D1R * D1L)

# Reaction kinetics or equilibrium
for J in range(1, L + 1):
    # Kinetics turned off
    # DC=DT*(KF*CRNEW(J)*CLNEW(J)-
KB*CRLNEW(J))

PHI = CLNEW[J] / (KD + CLNEW[J])
CT = CRNEW[J] + CRLNEW[J]
DC = PHI * CT - CRLNEW[J]

if DC > 0.05 * CLNEW[J]:
    DC = 0.1 * CLNEW[J]
if DC > 0.05 * CRNEW[J]:
    DC = 0.1 * CRNEW[J]
if (-1.0 * DC) > 0.05 * CRLNEW[J]:
    DC = -0.05 * CRLNEW[J]

```

```

CRNEW[J] = CRNEW[J] - DC
CLNEW[J] = CLNEW[J] - DC
CRLNEW[J] = CRLNEW[J] + DC

for J in range(1, L + 1):
    CROLD[J] = CRNEW[J]
    CLOLD[J] = CLNEW[J]
    CRLOLD[J] = CRLNEW[J]
    CRCOLD[J] = CRCNEW[J]

CRCOLDMAX = 0
CROLDMAX = 0
for K in range(1, L + 1):
    KR = K * DX * 1.0E+4
    T1 = CROLD[K]
    T2 = CRLOLD[K]
    T3 = CLOLD[K]
    T4 = CRCOLD[K]
    T5 = T1 + T2
    if T4 > CRCOLDMAX:
        KPMAX1 = KP
        CRCOLDMAX = T4
    if T5 > CROLDMAX:
        KPMAX2 = KP
        CROLDMAX = T5

# OUTPUT ROUTINE
list = [LW, TF, CRSTAR, CLSTAR, KD, DR, DL, DRL,
KPMAX2, KPMAX1]

indexs = ['Total channel width (cm)      ',
'Simulation time (s)                    ', 'Receptor
molecule concentration (M)'
, 'Ligand concentration (M) ',
'Dissociation constant KD (M)          ', 'Receptor
molecule D (cm2/s)                    ',
'Ligand molecule D (cm2/s)            ',
'Receptor-ligand complex D (cm2/s)    ', 'Max
with ligand                            ',
'Max without ligand                    ']
column = ['content']
test = pd.DataFrame(index=indexs, data=list,
columns=column)
test.to_csv('cs/test1.csv')
print('Total channel width (cm):        \n', LW)
print('Simulation time (s):              \n', TF)
f = open('cs/cav_file.csv', 'w', encoding='utf-
8', newline='')
csv_write = csv.writer(f)
csv_write.writerow(['d(um)', 'R', 'RL', 'L',
'Ro', 'Rtot'])
for K in range(1, L + 1):
    KR = K * DX * 1.0E+4
    T1 = CROLD[K]
    T2 = CRLOLD[K]
    T3 = CLOLD[K]
    T4 = CRCOLD[K]
    T5 = T1 + T2
    csv_write.writerow([KP, T1, T2, T3, T4, T5])
f.close()

```

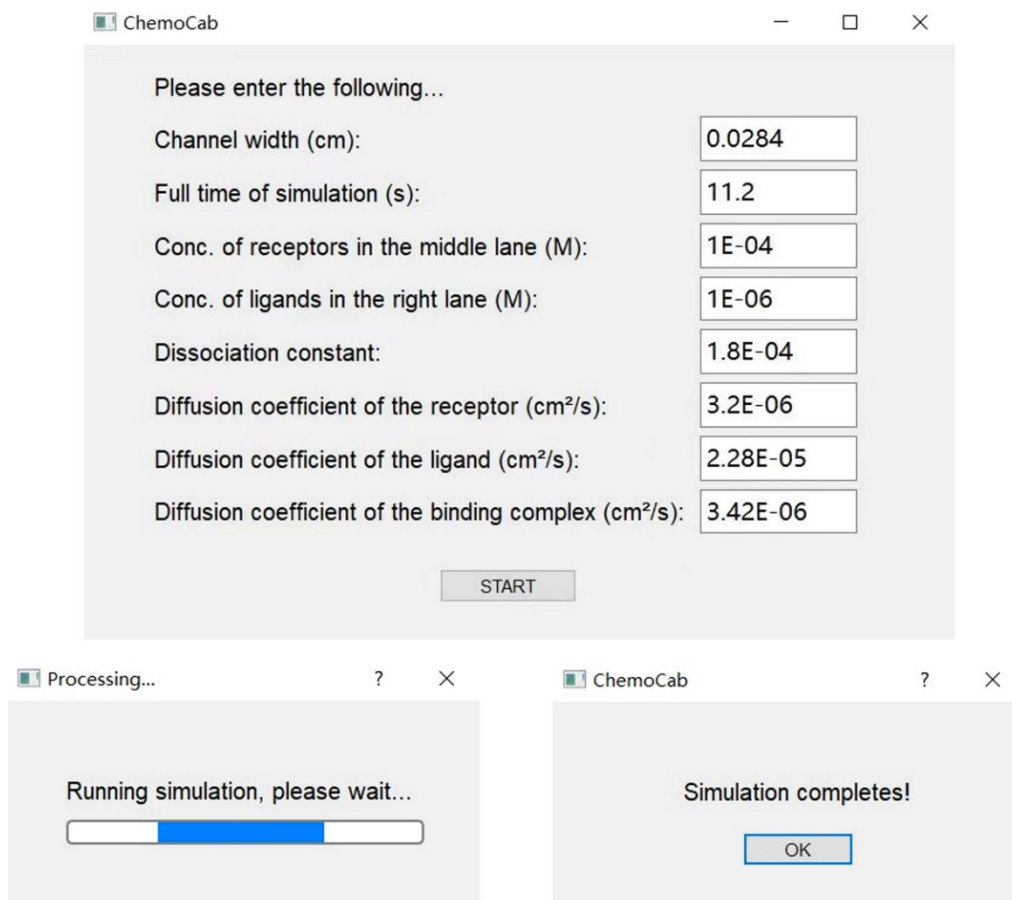
1 This program initialized with a handful of inputs tabulated in [Table S1](#):

2

**Table S1.** Parameters as initial conditions

Item	Value
Channel width ( $w$ ):	0.0284 cm
Full time of simulation ( $t$ ):	11.2 s
Concentration of receptors in the middle lane ( $c_R$ ):	$1.0 \times 10^{-4}$ M
Concentration of ligands in the right lane ( $c_L$ ):	0, $1.0 \times 10^{-9 \sim 0}$ M
Dissociation constant ( $K_D$ ):	$1.81 \times 10^{-3}$ M
Diffusion coefficient of the receptor ( $D_R$ ):	$3.27 \times 10^{-6}$ cm <sup>2</sup> /s
Diffusion coefficient of the ligand ( $D_L$ ):	$2.28 \times 10^{-5}$ cm <sup>2</sup> /s
Diffusion coefficient of the binding complex ( $D_{RL}$ ):	$3.46 \times 10^{-6}$ cm <sup>2</sup> /s

3



4

5

**Fig. S14** Compiled screenshots about user interface with pop-ups of operational dialogue.

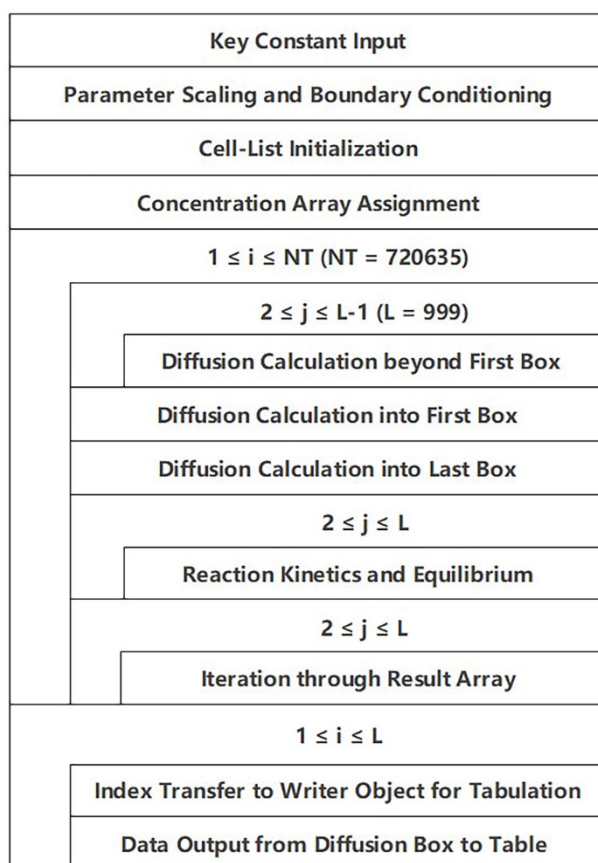


**Fig. S15** The Nassi-Schneiderman (N-S) flowchart of the code.

1

2

3

#### 4 Kernel Functions

5 Provided the ergodic principle, the 3D steady fluid flow can be reduced into one-dimensional  
6 case about the horizontal cross-section profile of the Probe concentration at certain  $x$ . Then  
7  $J_R(R)$  in Eq. 8 could be rewritten in a relatively concise way:

$$J_R(x) = -D_R \left[ \frac{dc_R(x)}{dx} - c_R(x) \cdot \frac{\Phi}{c_L(x)} \cdot \frac{dc_L(x)}{dx} \right] \quad (\text{S15})$$

8 Here,  $\Phi = c_{RL}(x)/c_{R_0}(x)$  deemed as the mole fraction of the complexed Probe molecule.

9 More importantly,

$$D_{Rb} = D_R \cdot \frac{K_A c_R(x)}{1 + K_A c_L(x)} = D_R \cdot \frac{c_{RL}(x)}{c_{R_0}(x)} \cdot \frac{c_R(x)}{c_L(x)} \quad (\text{S16})$$

10 which suggests that the artificial coefficient,  $D_{Rb}$ , phenomenologically correlates to **(1)** the  
11 mole fraction of complexed Probe molecule, and **(2)** the molar ratio of Probe vs. Ligand.

1 To track the time-dependent trajectory, iteration was implemented by making use of the  
 2 spatial derivative of  $J_R$  (Fick's Second Law):

$$\frac{dc_R(x)}{dt} = -\frac{dJ_R(x)}{dx} = D_R \left[ \frac{d^2c_R}{dx^2} - \frac{\Phi}{c_L} \left( c_R \cdot \frac{d^2c_L}{dx^2} + \frac{dc_R}{dx} \cdot \frac{dc_L}{dx} \right) \right] \quad (\text{S17})$$

3 This equation elucidates the strategy for updating  $c_P$  throughout the "cell list", its refreshing  
 4 speed (*i.e.* the time step) is scaled by the diffusion layer  $\sqrt{2D_R t}$ .

5 Simultaneously, the concentration gradient of Ligand ( $dJ_L(x)/dx$ ) would be perturbed  
 6 mutually. Rather than treating it with the assumption of sufficient dilution,<sup>[S11]</sup> the collective  
 7 motion of ligands would still conform to a similar cross-diffusion formalism as Eq. S12:

$$\frac{dc_L(x)}{dt} = -\frac{dJ_L(x)}{dx} = D_L \left[ \frac{d^2c_L}{dx^2} - \frac{\Phi}{c_R} \left( c_L \cdot \frac{d^2c_R}{dx^2} + \frac{dc_R}{dx} \cdot \frac{dc_L}{dx} \right) \right] \quad (\text{S18})$$

8 It is noteworthy that:

9 **1.** The fluctuation in viscosity is so little (*i.e.* ~6.8% difference) among aqueous solutions  
 10 with various Ligand concentrations, which has been validated in Fig. S16, that we neglected  
 11 its effect on the cross-channel diffusion.

12 **2.** The loop increment ( $\Delta c_R$ ) is introduced by making subtraction to renew the real-time  
 13 consumption of  $c_R(x)$  and  $c_L(x)$  and the formation of  $c_{RL}(x)$  in each cycle:

$$\Delta c = [c_R(x) + c_{RL}(x)] \cdot \frac{c_L(x)}{K_D + c_L(x)} - \frac{c_{R_0}(x) \cdot c_L(x)}{K_D + c_L(x)} \quad (\text{S19})$$

14 **3.** The program initializes with a comprehensive configuration of inputs, which are tabulated  
 15 in Table S1.

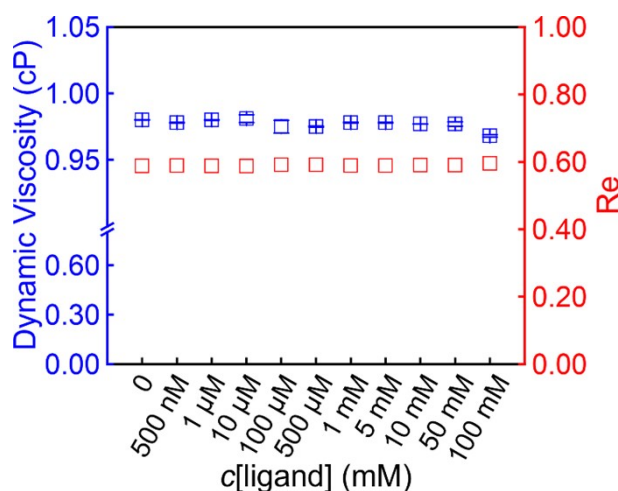
## 1 Viscosity and Reynolds Number Measurements

2 The viscosities of subject solutions were measured using a Ubbelohde tube (viscometer  
3 constant:  $0.003529 \text{ cSt}\cdot\text{s}^{-1}$ , Shanghai Chigao Instrument Co., Ltd.) that suspended upright  
4 under a stand holder in a cylindrical tank with  $25 \text{ }^\circ\text{C}$  water circulation. 2 mL of testing liquid  
5 was sucked up into the upper bulb and allowed to drain freely through the capillary. At least  
6 three successive repeats were done to time how long it took the meniscus to travel between two  
7 marks above and below the bulb respectively. Multiplying the effluxation in the variant of  
8 Poiseuille's law with the dynamic viscosity ( $\eta$ ) of methylcyclohexene (MCH,  $\eta = 0.980 \text{ CR}$  at  
9  $23 \text{ }^\circ\text{C}$ ) to make a conversion factor,<sup>[S5]</sup> the average  $\eta$  of test samples were scaled and  
10 summarized in Fig. S16.

11 To judge the Newtonian fluidity, the Reynolds number ( $Re$ ) was assessed by its definition  
12 with respect to the characteristic dimension of a rectangular duct:<sup>[S6]</sup>

$$Re = \frac{uL}{v} = \frac{2v\rho}{\eta(a+b)} \quad (\text{S20})$$

13 where  $u$  and  $v$  stand respectively for the maximum bulky and linear flow rate;  $L$  means the  
14 hydraulic diameter;  $\rho$  is the density;  $a$  and  $b$  are depth and width, respectively; and  $v$  is the  
15 kinematic viscosity ( $v = \eta/\rho$ ). In the situation of mere MCH, one would get a low  $Re = 0.603$ ,  
16 signifying that viscous forces are dominant in this laminar flow regime.



17

18 **Fig. S16** Dynamic viscosity (blue dots) and Reynold number (red) of MCH containing ZnTCPP-TOA at a  
19 constant  $100 \mu\text{M}$  and pyridine of variable concentrations from 0 to 100 mM at  $23 \text{ }^\circ\text{C}$ . The viscosities barely deviate  
20 from that of the blank solution ( $0.941 \text{ cP}$ ), which differs at most by just 2.8% from that has 100 mM pyridine  
21 ( $0.968 \text{ cP}$ ).

## 1 **References**

- 2 [S1] F. Helmich, C. C. Lee, M. M. Nieuwenhuizen, J. C. Gielen, P. C. Christianen, A. Larsen,  
3 G. Fytas, P. E. Leclère, A. P. Schenning and E. W. Meijer, *Angew. Chem. Int. Ed.* **2010**,  
4 *49*, 3939–3942.
- 5 [S2] F. Yang, X. Y. Liu and Z. J. Yang, *Angew. Chem. Int. Ed.* **2021**, *60*, 14671–14678.
- 6 [S3] J. G. Speight, *Lange's Handbook of Chemistry*. 17<sup>th</sup> Ed., New York, NY: McGraw-  
7 Hill Education, **2016**.
- 8 [S4] K. K. Dey, F. Y. Pong, J. Breffke, R. Pavlick, E. Hatzakis, C. Pacheco and A. Sen,  
9 *Angew. Chem. Int. Ed.* **2016**, *128*, 1125–1129.
- 10 [S5] N. D. Kondratyuk, V. V. Pisarev and J. P. Ewen, *J. Chem. Phys.* **2020**, *153*, 154502.
- 11 [S6] S. Shim, *Chem. Rev.* **2022**, *122*, 6986–7009.